AIP | Journal of Applied Physics

Optical gain characteristics of staggered InGaN quantum wells lasers

Hongping Zhao and Nelson Tansu

Citation: J. Appl. Phys. **107**, 113110 (2010); doi: 10.1063/1.3407564
View online: http://dx.doi.org/10.1063/1.3407564
View Table of Contents: http://jap.aip.org/resource/1/JAPIAU/v107/i11
Published by the American Institute of Physics.

Optical gain characteristics of staggered InGaN quantum wells lasers

Hongping Zhao[a] and Nelson Tansu[a]
Department of Electrical and Computer Engineering, Center for Optical Technologies, Lehigh University, 7 Asa Drive, Bethlehem, Pennsylvania 18015, USA

(Received 20 August 2009; accepted 24 March 2010; published online 9 June 2010)

Staggered InGaN quantum wells (QWs) are analyzed as improved gain media for laser diodes (LDs) lasing at 440 and 500 nm. The calculation of band structure is based on a 6-band $\boldsymbol{k}\cdot\boldsymbol{p}$ method taking into account the valence band mixing, strain effect, and spontaneous and piezoelectric polarizations as well as the carrier screening effect. Staggered InGaN QWs with two-layer and three-layer step-function like In-content InGaN QWs structures are investigated to enhance the optical gain as well as to reduce the threshold current density for LDs emitting at 440 and 500 nm. Our analysis shows that the optical gain is enhanced by 1.5–2.1 times by utilizing the staggered InGaN QW active region emitting at 440 nm, which leads to a reduction of the threshold current density up to 24% as compared to that of the conventional InGaN QW laser. Staggered InGaN QWs with enhanced optical gain shows significantly reduced blue-shift as carrier density increases, which enables nitride QWs with high optical gain in the green spectral regime. The use of green-emitting three-layer staggered InGaN QW is also expected to lead to reduction in the threshold carrier density by 30%. © *2010 American Institute of Physics*. [doi:10.1063/1.3407564]

I. INTRODUCTION

GaN and InGaN quantum wells (QWs) based laser diodes (LDs) with violet and blue emission wavelength have been successfully commercialized with relatively low threshold current density below 2 kA/cm^2.[1–3] However, the threshold current density for InGaN-based LDs is still significantly higher as compared to those of the InGaAs-based LDs ($J_{th} < 100-150\ A/cm^2$).[4,5] Major challenges preventing high performance conventional InGaN QWs LDs especially emitting longer than 480 nm include (1) phase separation in high In-content InGaN QW resulting in poor crystalline quality; (2) high strain misfit dislocation density leading to poor material quality and high nonradiative recombination rate, and (3) increased built-in electrostatic field due to the spontaneous and piezoelectric polarizations. The existence of the electric filed in the InGaN QW (Ref. 6) separates the electron and hole wave functions, which reduces the electron-hole wave function overlap (Γ_{e_hh}) as compared to the flat band lineups in InGaAs based QWs. The use of InGaN QWs with high In-content or thick QWs result in large internal electric field in the QW (Ref. 6) leading to low electron-hole wave function overlap (Γ_{e_hh}).

To extend the lasing wavelength of InGaN QWs LDs into the green spectral regime, either high In-content InGaN QW or thick InGaN QW is required for the active region. However, both approaches will lead to a significant reduction in the electron-hole wave function overlap (Γ_{e_hh}) due to the charge separation from the electric filed in the QWs. To avoid the challenges caused by the internal electric field in c-plane InGaN QW, InGaN QWs grown on nonpolar or semipolar substrate have been studied.[7–10] By removing or reducing the electric field in the QW, nonpolar, or semipolar InGaN QWs enhance the electron-hole wave function overlap (Γ_{e_hh}). However, to extend the emission wavelength of nonpolar or semipolar InGaN QW to the green regime, much higher In-content is required as compared to that of the c-plane InGaN QW, which presents a huge challenge for metal-organic chemical-vapor deposition (MOCVD) epitaxy due to the lattice mismatch between InGaN QW and GaN barriers and the additional challenges in growing high In-content InGaN alloy. Recently, several other approaches have been proposed to enhance the electron-hole wave function overlap (Γ_{e_hh}) for c-plane InGaN QWs, as follows: (1) embedded AlGaN δ-layer in InGaN QW,[11,12] (2) staggered InGaN QW,[13–22] (3) type-II InGaN–GaNAs QW,[23,24] (4) strain-compensated InGaN–AlGaN QW,[25,26] and (5) triangular InGaN QW.[27]

The concept of the two-layer staggered InGaN QWs as active regions for light-emitting diodes (LEDs) in the blue regime was proposed and demonstrated in Refs 12 and 13. The comprehensive theoretical studies of both two-layer and three-layer staggered InGaN QWs LEDs emitting in the green regime show 2.6–3.7 times enhancement in the radiative recombination rate as compared to that of the conventional InGaN QW.[16] Experimental demonstration of the three-layer staggered InGaN QWs LEDs emitting at 520–525 nm shows the enhancement of the output power of 2–3.5 times as compared to that of the conventional InGaN QWs LEDs.[17] Theoretical studies of the staggered InGaN QWs for LEDs devices by employing many-body Coulomb effect were reported,[19–21] and the results also exhibited similar enhancement factor in radiative recombination rate and radiative efficiency. In contrast to the studies of the staggered InGaN QWs for LEDs,[13–22] there has been no prior works on the comprehensive studies of the gain characteristics of the staggered InGaN QWs as active region for lasers.

In this paper, we present a comprehensive analysis on the optical gain and threshold current density characteristics of staggered c-plane InGaN QWs emitting at 440 and 500

[a]Electronic addresses: hoz207@lehigh.edu and tansu@lehigh.edu.

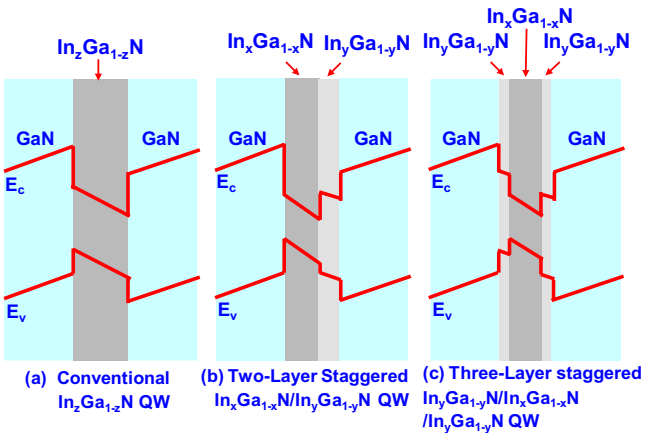

FIG. 1. (Color online) Schematics of the (a) conventional $In_zGa_{1-z}N-GaN$ QW; (b) two-layer staggered $In_xGa_{1-x}N/In_yGa_{1-y}N$ QW; and (c) three-layer staggered $In_yGa_{1-y}N/In_xGa_{1-x}N/In_yGa_{1-y}N$ QW structures.

nm. Both two-layer ($In_xGa_{1-x}N/In_yGa_{1-y}N$) and three-layer ($In_yGa_{1-y}N/In_xGa_{1-x}N/In_yGa_{1-y}N$) staggered InGaN QWs with step-function like In-content profile are analyzed as improved gain media with enhanced electron-hole wave function overlap (Γ_{e_hh}). In this analysis, the band structures are calculated based on a 6-band $\boldsymbol{k}\cdot\boldsymbol{p}$ method taking into account the valence band mixing, strain effect, spontaneous, and piezoelectric polarizations as well as the carrier screening effect.[26,28–30] Spontaneous emission radiative recombination rate and optical gain are analyzed and compared for both conventional and staggered InGaN QWs. The gain characteristics for staggered InGaN QWs are analyzed for both 440 and 500 nm spectral regimes. Threshold characteristics and optimization for staggered InGaN QWs emitting at 440 and 500 nm are calculated and analyzed.

II. CONCEPT OF STAGGERED InGaN QW

The existence of electrostatic field in the InGaN QW results in "charge separation" effect in the QW, which leads to spatial separation of the electron and hole wave functions in the QW. The charge separation in conventional InGaN QW leads to a severe reduction of the electron-hole wave function overlap (Γ_{e_hh}). The low electron-hole wave function overlap (Γ_{e_hh}) in conventional InGaN QWs active region leads to significant reduction in optical gain for nitride lasers, in particular as the emission wavelength is extended to the green spectral regime. The use of staggered InGaN QW design is to enhance the electron-hole wave function overlap (Γ_{e_hh}) by engineering the band lineups of the InGaN QW, hence leading to increase in the optical gain of the QW for laser applications.

In this work, three QW structures are studied and compared as follows: (a) the conventional $In_zGa_{1-z}N$ QW; (b) the two-layer staggered $In_xGa_{1-x}N/In_yGa_{1-y}N$ QW, and (c) the three-layer staggered $In_yGa_{1-y}N/In_xGa_{1-x}N/In_yGa_{1-y}N$ QW structures, which are surrounded by GaN barrier layers as shown in Fig. 1. Note that the three structures have the same total QW thickness (d_{QW}) for comparison purpose. The conventional $In_zGa_{1-z}N$ QW contains uniform In-content (z) with the QW thickness of d_{QW}. The two-layer staggered $In_xGa_{1-x}N/In_yGa_{1-y}N$ QW is characterized by the use of a step-function like In-content profile in the QW as follows: (1) high In-content of x with thickness of d_{w1}, and (2) lower In-content of y with thickness of d_{w2}, where $d_{w1}+d_{w2}=d_{QW}$. In contrast to the two-layer staggered InGaN QW, the three-layer staggered $In_yGa_{1-y}N/In_xGa_{1-x}N/In_yGa_{1-y}N$ QW contains the higher In-content (x) sublayer in the center, which is sandwiched between two InGaN sub-layers with lower In-content of y. The total thickness (d_{QW}) of the three-layer staggered InGaN QW is also designed as equal to $d_{QW}=d_{w1}+d_{w2}+d_{w3}$. To compare the performance of the active regions of these three structures for laser application, the In-contents and sublayer thickness for the conventional InGaN QW, two-layer staggered $In_xGa_{1-x}N/In_yGa_{1-y}N$ QW and three-layer staggered $In_yGa_{1-y}N/In_xGa_{1-x}N/In_yGa_{1-y}N$ QW are designed such that all three QWs emit at similar lasing wavelengths. The designs of the staggered InGaN QW structures for 440 nm emitting lasers will be presented in Sec. IV, and the staggered InGaN QW structures for 500 nm spectral regimes will be presented in Sec. V.

Note that the designs of the 3-layer staggered InGaN QWs emitting in blue and green spectral regimes employ very thin InGaN sublayers (5–6 Å), which may potentially lead to growth challenges by MOCVD in particular to achieve abrupt interface. However, even for less abrupt interfaces in InGaN/InGaN heterostructure layers in the staggered InGaN QW, the electron-hole wave function overlap can be enhanced resulting in improved radiative recombination rate. Recent experiments on MOCVD-grown 3-layer staggered InGaN QWs LEDs emitting in the green spectral regime show significant enhancement in output power and efficiency from electrically-injected devices.[17,18]

III. THEORETICAL AND NUMERICAL MODEL

The band structures and wave functions are obtained by utilizing a self-consistent 6-band $\boldsymbol{k}\cdot\boldsymbol{p}$ method for wurtzite semiconductor.[28–30] To take into consideration of the carrier screening effect, the Schrödinger equations and Poisson equations are solved self-consistently till the eigen energies converge.[26,28–30] The convergence condition for this calculation is set such that the tolerance of the eigen energies is less than 0.1%. To calculate the heterostructure/nanostructure, finite difference method is used to solve the 6×6 $\boldsymbol{k}\cdot\boldsymbol{p}$ Hamiltonian matrix with the step size of 1 Å. The details of the formalism for the self-consistent 6-band $\boldsymbol{k}\cdot\boldsymbol{p}$ are presented in Refs. 26 and 28–30. The parameters for the InN and GaN are taken from Refs. 31 and 32, which are summarized in the table in Ref. 26.

The spontaneous emission radiative recombination rate is proportional to the square of the momentum matrix element $[(M)^2_{nm}(k_t)]$.[26] The spontaneous emission rate is obtained by taking into account all possible transitions between n^{th} conduction subbands and m^{th} valence subbands as follows

$$r^{spon}(\hbar\omega) = \frac{2q^2\pi}{n_r c\varepsilon_0 m_0^2 \omega L_\omega} \sum_{\sigma=U,L} \sum_{n,m} \int \frac{k_t dk_t}{2\pi} |(M)_{nm}(k_t)|^2 \cdot \frac{f_n^c(k_t)[1-f_{\sigma m}^v(k_t)](\gamma/\pi)}{[E_{\sigma,nm}^{cv}(k_t)-\hbar\omega]^2+\gamma^2}, \quad (1)$$

where $(M)_{nm}(k_t)$ is the momentum matrix element between n^{th} conduction subband and m^{th} valence subband, which is a function of the in-plane wave vector k_t. The parameter L_ω is the thickness of the QW, and $f_n^c(k_t)$ and $f_{\sigma m}^v(k_t)$ are the Fermi–Dirac distribution functions for the electrons in conduction band and valence band. The detail of the derivation of Eq. (1) was presented in Ref. 26. The existence of the electric field in the QW leads to the band bending of the potential edge for both conduction band and valence band, which allows the transition between the states with unequal quantum numbers ($m \neq n$). In this calculation, all possible transitions between the confined states of the conduction band and valence band are taken into account.

The total spontaneous emission radiative recombination rate per unit volume (s^{-1} cm^{-3}) is obtained by integrating the Eq. (1) over the entire energy range as follows

$$R_{sp} = \int_0^\infty r^{spon}(\hbar\omega) d(\hbar\omega). \quad (2)$$

Based on Eq. (1), the optical gain for III-Nitride semiconductors is related to the spontaneous emission as follows

$$g(\hbar\omega) = r^{spon}(\hbar\omega)\left[1-\exp\left(\frac{\hbar\omega-\Delta F}{k_B T}\right)\right], \quad (3)$$

where ΔF is separation of the quasi-Fermi levels of electrons (F_C) and holes (F_V).

The equations presented here will be used to calculate the band structure, the spontaneous emission radiative recombination rate and optical gain for InGaN QWs. The details of the derivation and formulation of the simulation approach are presented in Ref. 26.

IV. OPTIMIZATION OF STAGGERED InGaN QWs LASERS AT 440-nm

A. Staggered InGaN QWs design for blue-emitting lasers

In this section, the optimization studies for staggered InGaN QW for lasers emitting in the 440 nm spectral regime are discussed. The following three QW structures are calculated and compared: (a) conventional 24-Å $In_{0.22}Ga_{0.78}N$ QW, (b) two-layer staggered 12-Å $In_{0.28}Ga_{0.72}N$/12-Å $In_{0.12}Ga_{0.88}N$ QW and (c) three-layer staggered 6-Å $In_{0.12}Ga_{0.88}N$/12-Å $In_{0.28}Ga_{0.72}N$/6-Å $In_{0.12}Ga_{0.88}N$ QW. The staggered InGaN QW structures are designed such that the two-layer staggered InGaN QW and three-layer staggered InGaN QW contain the same In-contents for the sublayers with relatively similar lasing wavelength at 435–440 nm. The electron-hole wave function overlaps (Γ_{e_hh}) for the two-layer staggered InGaN QW and three-layer staggered InGaN QW are 40.3% and 47.9%, respectively. As comparison, the electron-hole wave function overlap (Γ_{e_hh}) for conventional 24-Å $In_{0.22}Ga_{0.78}N$ QW is 30%.

Based on Fermi's Golden Rule, the interband transition rate is proportional to the square of their electron-hole wave function overlap Γ_{e_hh}. By engineering the energy band lineups utilizing the two-layer and three-layer staggered InGaN QWs, the electron-hole wave function overlaps (Γ_{e_hh}) of these blue-emitting staggered InGaN QWs are improved by 1.34–1.6 times as compared to that of the conventional InGaN QW.

B. Momentum matrix elements characteristics

The momentum matrix element $[(M)_{nm}(k_t)]$ of InGaN QW is related to the electron-hole wave function overlap (Γ_{e_hh}). The expressions of the momentum matrix elements for transverse-electric (TE) and transverse-magnetic (TM) polarizations were derived in Ref. 26. Due to the compressive strain in the InGaN QW, the momentum matrix element with the TM polarization is much smaller than the one with the TE polarization. Thus, in this section, the momentum matrix elements with TE polarization for the conventional and staggered InGaN QWs are calculated and compared.

Figures 2(a)–2(c) show the dispersion relation of the square of the momentum matrix element for TE-polarization as a function of the in-plane wave vector k_t for conventional 24-Å $In_{0.22}Ga_{0.78}N$ QW [Fig. 2(a)], two-layer staggered 12-Å $In_{0.28}Ga_{0.72}N$/12-Å $In_{0.12}Ga_{0.88}N$ QW [Fig. 2(b)], and three-layer staggered 6-Å $In_{0.12}Ga_{0.88}N$/12-Å $In_{0.28}Ga_{0.72}N$/6-Å $In_{0.12}Ga_{0.88}N$ QW [Fig. 2(c)] with transitions between C1-HH1, C1-LH1, C1-HH2, C1-LH2, C2-HH1, C2-LH1, C2-HH2, and C2-LH2 at carrier density of $n=3\times10^{19}$ cm^{-3}. Note that the major contributions of the momentum matrix elements to the spontaneous emission and material gain are transitions between C1-HH1 and C1-LH1. By comparing Figs. 2(a)–2(c), the C1-HH1 and C1-LH1 transition matrix elements for the three-layer staggered InGaN QW are larger than those of the two-layer staggered InGaN QW, which is larger than that of the conventional InGaN QW.

The characteristics of the square of the momentum matrix elements $((M)_{nm}^2(k_t))$ at $k_t=0$ as a function of the carrier density were analyzed for $n=1\times10^{19}$ cm^{-3} up to $n=6\times10^{19}$ cm^{-3}. Note that the momentum matrix element at $k_t=0$ for the conduction band and heavy hole subband (C-HH) transition is similar to that of the conduction band and light hole subband (C-LH) transition. The momentum matrix elements of the major transitions between the conduction band and valence band (C1-HH1 and C1-LH1) increase as the carrier density increases. The C1-HH1 and C1-LH1 matrix elements for the three-layer staggered InGaN QW are larger than those of the two-layer staggered InGaN QW, and both staggered InGaN QWs have higher C1-HH1 and C1-LH1 matrix elements than those of the conventional InGaN QW.

C. Optical gain characteristics

Figure 3 shows the optical gain spectra for the conventional InGaN QW (dashed-dotted line), two-layer staggered InGaN QW (dashed line) and three-layer staggered InGaN QW (solid line) at carrier densities of 3×10^{19} and 5×10^{19} cm^{-3} at T=300 K. The staggered InGaN QWs exhibit improved optical gain as compared to the conventional

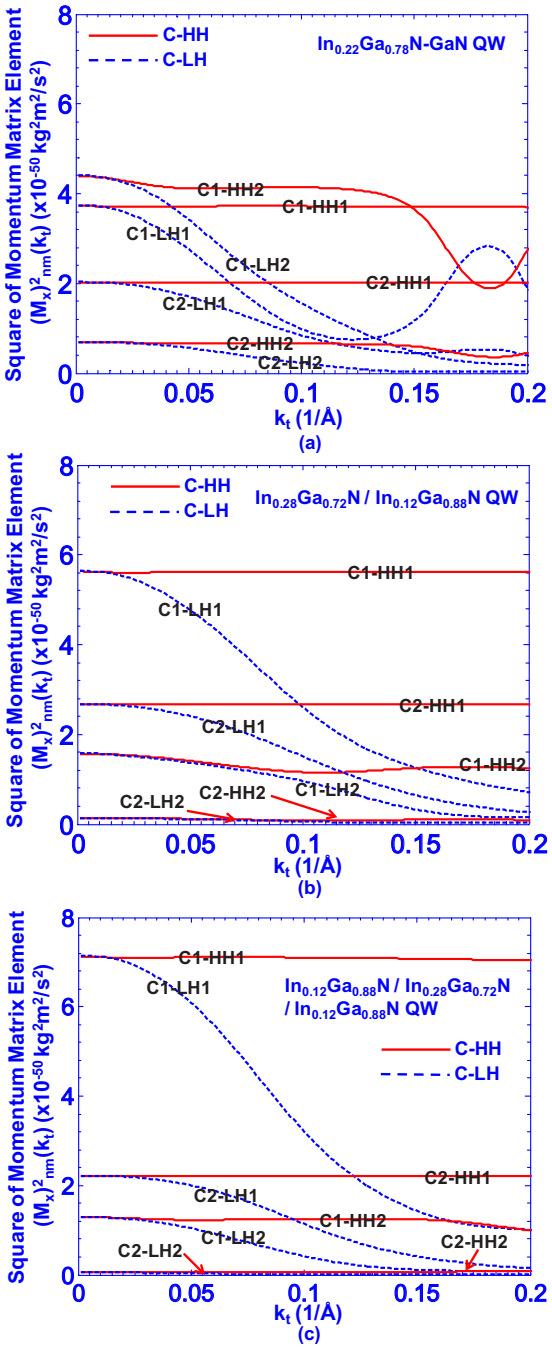

FIG. 2. (Color online) Square of momentum matrix elements as a function of the in-plane wave vector k_t in the TE-polarization for (a) conventional 24-Å $In_{0.22}Ga_{0.78}N$ QW, (b) two-layer staggered 12-Å $In_{0.28}Ga_{0.72}N$/12-Å $In_{0.12}Ga_{0.88}N$ QW and (c) three-layer staggered 6-Å $In_{0.12}Ga_{0.88}N$/12-Å $In_{0.28}Ga_{0.72}N$/6-Å $In_{0.12}Ga_{0.88}N$ QW at carrier density of 3×10^{19} cm^{-3}.

InGaN QW. At $n=5\times10^{19}$ cm^{-3}, the peak gain (g_p) for the two-layer staggered InGaN QW is 2710 cm^{-1}, which is 1.34 times of that of the conventional InGaN QW (2030 cm^{-1}), while the three-layer staggered InGaN QW shows 1.61 times improvement with the peak gain of 3270 cm^{-1}.

Figure 4 shows the peak material gain as a function of the carrier density up to 6×10^{19} cm^{-3}. A significant enhancement of the peak gain (g_p) by utilizing the staggered InGaN QW structures is observed in Fig. 4, which is important to reduce the threshold carrier density and threshold current density for the InGaN based LDs. The two-layer staggered InGaN QW shows 1.27–1.73 times enhancement as compared to the conventional InGaN QW, while the three-layer staggered InGaN QW shows 1.48–2.33 times enhancement in comparison to that of conventional InGaN QW. Note from Fig. 4, the optical gain and differential gain of staggered InGaN QW are significantly enhanced, which leads to significantly lower threshold carrier density (n_{th}) for laser application. Note that the three QW structures studied here have similar transparency carrier density (n_{tr}) $\sim 1.8\times10^{19}$ cm^{-3}.

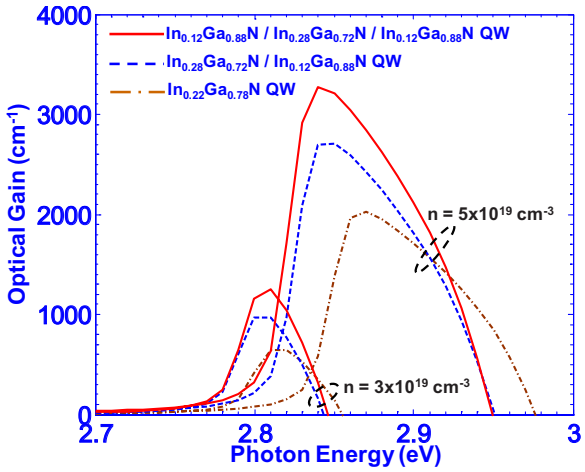

FIG. 3. (Color online) Optical gain spectra for conventional 24-Å $In_{0.22}Ga_{0.78}N$ QW, two-layer staggered 12-Å $In_{0.28}Ga_{0.72}N$/12-Å $In_{0.12}Ga_{0.88}N$ QW and three-layer staggered 6-Å $In_{0.12}Ga_{0.88}N$/12-Å $In_{0.28}Ga_{0.72}N$/6-Å $In_{0.12}Ga_{0.88}N$ QW emitting at ~440-nm for increasing carrier density $n=3-5\times10^{19}$ cm^{-3}.

Figure 5 shows the peak emission wavelength versus the optical gain for the conventional 24-Å $In_{0.22}Ga_{0.78}N$ QW, the two-layer staggered 12-Å $In_{0.28}Ga_{0.72}N$/12-Å $In_{0.12}Ga_{0.88}N$ QW and the three-layer staggered 6-Å $In_{0.12}Ga_{0.88}N$/12-Å $In_{0.28}Ga_{0.72}N$/6-Å $In_{0.12}Ga_{0.88}N$ QW. The peak emission wavelengths show blueshifts for increasing carrier density in the QW due to the carrier screening effect. Similarly, the blue-shifts in emission wavelengths are observed for increas-

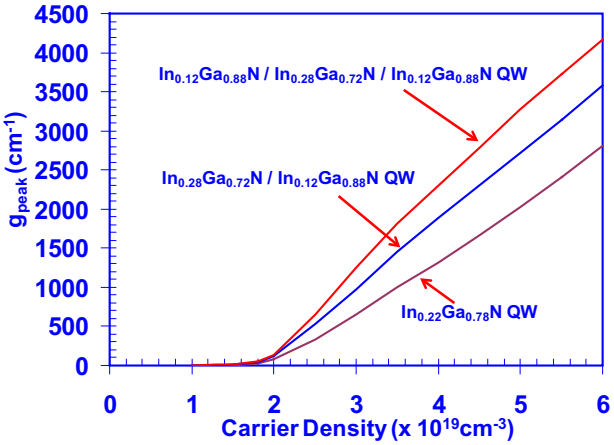

FIG. 4. (Color online) Peak optical material gain (g_p) as a function of carrier density for conventional 24-Å $In_{0.22}Ga_{0.78}N$ QW, two-layer staggered 12-Å $In_{0.28}Ga_{0.72}N$/12-Å $In_{0.12}Ga_{0.88}N$ QW and three-layer staggered 6-Å $In_{0.12}Ga_{0.88}N$/12-Å $In_{0.28}Ga_{0.72}N$/6-Å $In_{0.12}Ga_{0.88}N$ QW at room temperature.

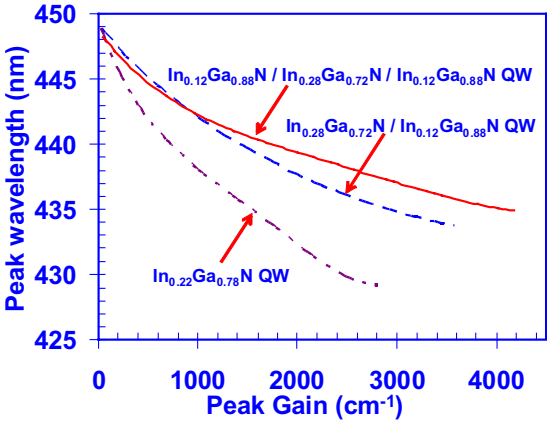

FIG. 5. (Color online) Peak emission wavelengths from gain spectra as a function of material gains for conventional 24-Å $In_{0.22}Ga_{0.78}N$ QW, two-layer staggered 12-Å $In_{0.28}Ga_{0.72}N$/12-Å $In_{0.12}Ga_{0.88}N$ QW and three-layer staggered 6-Å $In_{0.12}Ga_{0.88}N$/12-Å $In_{0.28}Ga_{0.72}N$/6-Å $In_{0.12}Ga_{0.88}N$ QW.

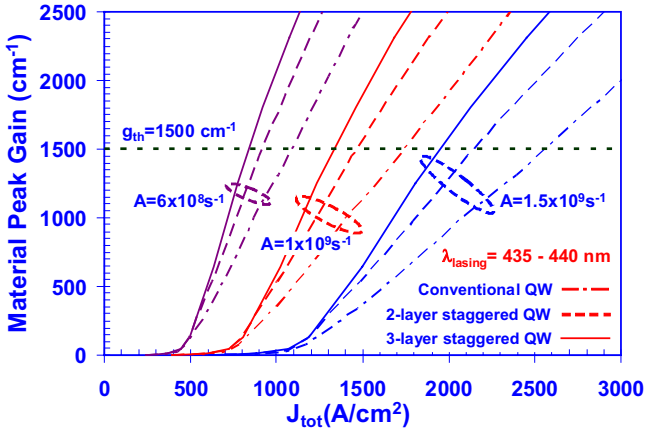

FIG. 6. (Color online) Material gain as a function of total current density for conventional 24-Å $In_{0.22}Ga_{0.78}N$ QW, two-layer staggered 12-Å $In_{0.28}Ga_{0.72}N$/12-Å $In_{0.12}Ga_{0.88}N$ QW and three-layer staggered 6-Å $In_{0.12}Ga_{0.88}N$/12-Å $In_{0.28}Ga_{0.72}N$/6-Å $In_{0.12}Ga_{0.88}N$ QW with monomolecular recombination rate of $A=6\times10^8$ s^{-1}, 1×10^9 s^{-1}, and 1.5×10^9 s^{-1}.

ing peak material gain in the QW. However, the blueshift observed in three-layer (and two-layer) staggered InGaN QW is ~9 nm (and ~11 nm) for material gain at 2000 cm^{-1}, which is significantly less in comparison to that (~17 nm) of the conventional InGaN QW.

D. Threshold current density characteristics

To study the feasibility of the conventional InGaN QW for LDs application, a laser structure with single QW as active region was employed in this analysis similar to the structure described in Ref. 3. The optical confinement (Γ_{opt}) and internal loss (α_i) are 0.01 and 8.6 cm^{-1}, respectively. The laser cavity length is assumed as 650 μm^{-1} with end-facet reflectivities of 95% and 56%, which corresponds to mirror loss (α_m) of 4.85 cm^{-1}. By using the equation $\Gamma_{opt}g_{th}=\alpha_i+\alpha_m$, the threshold gain ($g_{th}$) required for lasing is estimated as $g_{th}\sim1500$ cm^{-1}.

Note that for laser structure with threshold gain $g_{th}\sim1500$ cm^{-1}, the lasing wavelength for the two-layer (three-layer) staggered InGaN QW is ~439.5 nm (~440.5 nm), while the lasing wavelength for the conventional InGaN QW is ~435 nm. The slightly-longer lasing wavelength from the use of staggered InGaN QWs is due to the enhanced electron-hole wave function overlap (Γ_{e_hh}) and improved optical gain.

As shown in Fig. 5, the conventional InGaN QW requires much higher threshold carrier density ($n_{th}=4.23\times10^{19}$ cm^{-3}) to reach the lasing condition of $g_{th}=1500$ cm^{-1}. The two-layer staggered InGaN QW requires lower threshold carrier density of $n_{th}=3.6\times10^{19}$ cm^{-3}, while the threshold carrier density of three-layer staggered is reduced significantly to $n_{th}=3.2\times10^{19}$ cm^{-3}. Note that the lower threshold carrier density also leads to reduction in carrier screening effect, thus the lasing wavelengths for the staggered InGaN QWs are slightly longer than that of the conventional InGaN QW.

The threshold current densities are calculated for conventional InGaN QW, two-layer staggered InGaN QW, and three-layer staggered InGaN QW. The threshold current density is composed of two parts: the radiative current density (J_{rad}) and the nonradiative current density (J_{nr}). In this analysis, the monomolecular current density ($J_{mono}=A\cdot n$) is considered as the dominant component for the nonradiative current density, where A is the monomolecular recombination coefficient. For wide band gap material, the Auger recombination process is negligible due to the small value of the Auger recombination rate ($C_{Auger}<10^{-32}$ cm^6/sec).[33,34]

Figure 6 shows the peak gain (g_p) as a function of the total threshold current density ($J_{tot}=J_{rad}+J_{nr}$) for the conventional 24-Å $In_{0.22}Ga_{0.78}N$, two-layer staggered 12-Å $In_{0.28}Ga_{0.72}N$/12-Å $In_{0.12}Ga_{0.88}N$ QW and three-layer staggered 6-Å $In_{0.12}Ga_{0.88}N$/12-Å $In_{0.28}Ga_{0.72}N$/6-Å $In_{0.12}Ga_{0.88}N$ QW with three different monomolecular recombination rates ($A=6\times10^8$ s^{-1}, $A=1\times10^9$ s^{-1}, and A

TABLE I. Total threshold current densities (J_{th_total}) for conventional InGaN QW (24-Å $In_{0.22}Ga_{0.78}N$), two-layer staggered InGaN QW (12-Å $In_{0.28}Ga_{0.72}N$/12-Å $In_{0.12}Ga_{0.88}N$) and three-layer staggered InGaN QW (6-Å $In_{0.12}Ga_{0.88}N$/12-Å $In_{0.28}Ga_{0.72}N$/6-Å $In_{0.12}Ga_{0.88}N$ QW) with various monomolecular recombination rates (A). The laser devices were designed for lasing wavelength at 435–440 nm.

	Total threshold current density (J_{th_total}) (A/cm^2)		
Monomolecular recombination coefficient (A)	Conventional InGaN QW	Two-layer staggered InGaN QW	Three-layer staggered InGaN QW
$A=6\times10^8$ s^{-1}	1090	905	830
$A=1\times10^9$ s^{-1}	1730	1460	1320
$A=1.5\times10^9$ s^{-1}	2550	2150	1950
Lasing Wavelength	435 nm	439.5 nm	440.5 nm

$=1.5\times10^{9}$ s^{-1}), similar to the values used in Ref. 35. To achieve the threshold lasing condition ($g_{th}=1500$ cm^{-1}), the required total threshold current densities for the conventional InGaN QW, two-layer staggered InGaN QW and three-layer staggered InGaN QW for three different monomolecular recombination rate are shown in Table I. The threshold current density for the three-layer (or two-layer) staggered InGaN QW is calculated as 23.5%–23.8% (15.7%–17%) lower than that of the conventional InGaN QW. The reduction in threshold carrier density in staggered InGaN QW is important to suppress the nonradiative current density (J_{nr}), which in turn leads to suppression of total threshold current density ($J_{tot}=J_{rad}+J_{nr}$). The use of staggered InGaN QW as the active regions for blue-emitting lasers has the potential for reducing the threshold current density, which in turns leads to improved reliability for the laser devices.

It is important to note that there exists a large discrepancy on the Auger recombination coefficients of InGaN QW reported in the literature.[33,34,36,37] Recent theoretical studies predicted Auger recombination coefficients in InGaN QW structures as in the range of $C_{Auger}=3.5\times10^{-34}$ cm^6/sec (Ref. 33) up to $C_{Auger}=0.9-1\times10^{-32}$ cm^6/sec.[34] However, recent studies have indicated the possibility that the Auger recombination coefficient for thick InGaN/GaN double heterostructure active regions ($d_{Active}=10-77$ nm) and bulk InGaN as in the range of $C_{Auger}=1.4-2\times10^{-30}$ cm^6/sec.[36,37] Further studies are still required to clarify and confirm the Auger coefficients (C_{Auger}) for InGaN/GaN QW system, due to the large discrepancies from the reported Auger coefficients in the literature.[33,34,36,37] A significant reduction in threshold carrier density (n_{th}) achievable in the staggered InGaN QW will be crucial for suppressing the J_{Auger}, as the J_{Auger} is proportional to n_{th}^3. The reduction in the threshold carrier density due to the use of two-layer (or three-layer) staggered InGaN QW will correspond to 38.3% (or 56.7%) reduction in Auger current density at threshold (J_{th_Auger}).

V. STAGGERED InGaN QWs LASERS AT 500-nm

A. Current status of green-emitting InGaN QWs lasers

The green-emitting InGaN QW lasers attract large interest due to its applications for the replacement of gas lasers, laser projection, and biomedical applications. Recently, InGaN QW based LDs grown on c-plane GaN substrate with lasing wavelength of 510–515 nm was demonstrated by Nichia with threshold current density of 4.4 kA/cm^2 at 25 °C and output power of 5 mW (at $I=88$ mA and $V=5.5$ V).[38] Note that the laser structure[38] was fabricated by employing both facets coated with high reflectivity (HR) dielectric films (HR/HR), which reduces the mirror loss and threshold gain. However, the HR/HR coatings on both facets limit the output power and external differential quantum efficiency of LDs, which leads to limitation of conventional InGaN QW as active regions for high-power LDs or other laser devices requiring high gain active region (i.e., VCSELs). Recently, OSRAM reported the 500 nm electrically driven InGaN based LDs grown on c-plane GaN substrate with threshold current density of 8.2 kA/cm^2 and output power of several tens of miliwatts.[39] The laser cavity described in Ref. 39 was fabricated with mirror coatings of 50% and 95%. It is very challenging to extend the conventional InGaN QW based LDs to the green spectral regime with high output power and low-threshold current density.

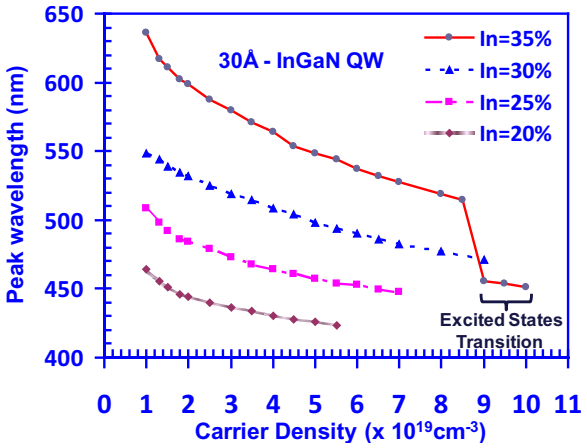

FIG. 7. (Color online) Peak emission wavelength from gain spectra as a function of carrier density for four different conventional 30-Å InGaN QWs with varied In-content of 25%, 30%, 35%, and 40%.

Further advances are still required to reduce the threshold current density from 4.4–8.2 kA/cm^2 down to more acceptable level. Significant reduction in threshold current density in green-emitting diode lasers are important, in particular for enabling the nitride QW lasers as practical and reliable laser technology in the green spectral regimes.

B. Challenges of conventional InGaN QW for green LDs

In this section, the issues on the QW design for green-emitting nitride lasers based on conventional design will be discussed. To achieve extension of lasing wavelength into the green spectral regime, the QW structure needs to be designed with slightly thicker QW dimension ($d_{QW}\sim3$ nm) and higher In-content (In$\sim$30%). To systematically study the relationship between the peak gain emission wavelength and the carrier density, four conventional InGaN QWs with the same QW thickness of 30-Å are compared for various In-contents of 20%, 25%, 30%, and 35% (as shown in Fig. 7). As the carrier density increases, the emission wavelengths of the peak gain show blueshifts for all the four conventional InGaN QW structures due to the carrier screening effect. For the case of conventional 30-Å $In_{0.35}Ga_{0.65}N$ QW, the excited states transition becomes the dominant peak gain transition, instead of the ground states transition, due to the carrier filling effect for the case of high carrier density above 9×10^{19} cm^{-3}.

To illustrate the excited states transition phenomena clearly, Fig. 8 shows the optical gain spectra versus the photon energy for the conventional 30-Å $In_{0.35}Ga_{0.65}N$ QW with carrier density from $n=6\times10^{19}$ cm^{-3} up to $n=10\times10^{19}$ cm^{-3}. Note that the second peak of the optical gain spectrum appears at $n=8\times10^{19}$ cm^{-3}, as shown in Fig. 8. The second peak become dominant as the carrier density increases further ($n=9\times10^{19}$ cm^{-3} and $n=10\times10^{19}$ cm^{-3}),

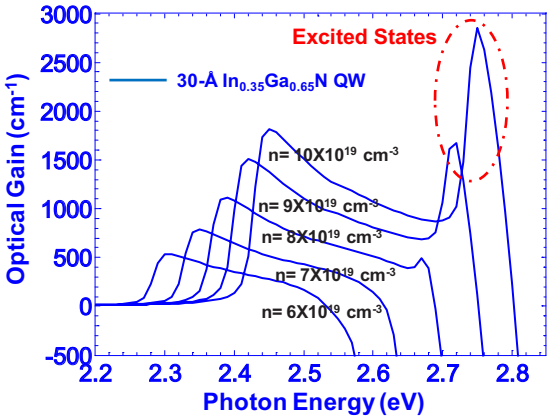

FIG. 8. (Color online) Optical gain spectra for conventional 30-Å $In_{0.35}Ga_{0.65}N$ QW with carrier density up to $n=10\times10^{19}$ cm^{-3}.

which makes it challenging to push the lasing wavelength to green emission just by employing conventional InGaN QW as the laser active region. The phenomenon of broadening of the gain spectra and excited state electroluminescence spectra due to band filling effects from excited state transition at high carrier density in InGaN QW have also been reported,[40,41] in particular, for InGaN QW structures with wider dimension and low momentum matrix element. The gain spectra broadening due to band filling effect from excited state transitions at high carrier density was commonly observed in QW structures with low momentum matrix elements,[42,43] resulting in excited states transition contributing to dominant gain peak at high carrier injection.[42,43]

Figure 9 shows the peak emission wavelengths versus the peak optical gains for the four conventional 30-Å InGaN QWs with varied In-contents (20%, 25%, 30%, and 35%). Similar with Fig. 7, the emission wavelength shows blueshift as the optical gain increases due to the carrier screening effect. Note that the conventional InGaN QW structures with higher In-contents show significantly more pronounced blueshift as compared to the structures with lower In-content, which is expected from the lower electron-hole wave function overlap and differential gain of the higher In-content QW structures. For laser structures with threshold gain $(g_{th})\sim1500$ cm^{-1}, the longest lasing wavelength for the

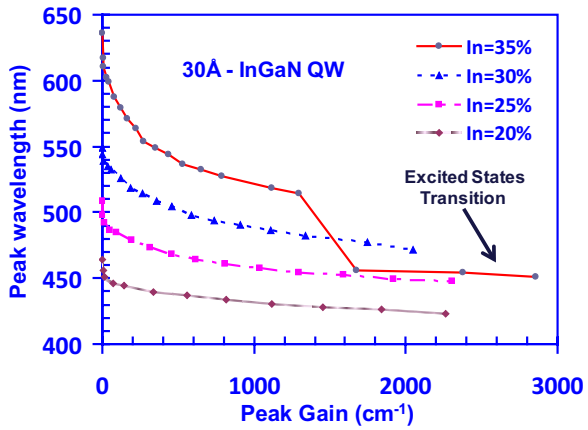

FIG. 9. (Color online) Peak emission wavelength from gain spectra as a function of material gain for four different conventional 30-Å InGaN QWs with varied In-content of 25%, 30%, 35%, and 40%.

conventional 30-Å InGaN QWs studied here with various In-contents is ~480 nm. There are two factors that lead to the challenges and limitations for extending the conventional InGaN QWs for achieving lasing wavelength into green regime: (1) the requirement of high threshold carrier density from this QW structure due to the low electron-hole wave function overlap (Γ_{e_hh}), which results in significant blueshift from the carrier screening effect (2) the strong band filling effect at high carrier density for conventional InGaN QW structure with reduced optical matrix element. Thus, it is challenging to achieve low-threshold and high performance nitride laser devices emitting in the green spectral regime, by only employing conventional InGaN QW as laser active region.

To resolve the fundamental issue for the conventional InGaN QW based LDs due to the low electron-hole wave function overlap (Γ_{e_hh}), novel structures with enhanced overlap Γ_{e_hh} is important to achieve low-threshold nitride diode lasers emitting in the green spectral regime or beyond. By employing nitride QW with improved Γ_{e_hh} (such as staggered InGaN QW), several important design considerations for green-emitting InGaN QW can be achieved as follows: (1) reduction in threshold carrier density and (2) significant reduction in blue shift of the lasing wavelength due to the less carrier screening effect. The reduction in threshold carrier density is important, as this will lead to reductions in non-radiative recombination threshold current density and band filling effect.

C. Spontaneous emission and optical gain of staggered InGaN QWs lasers at 500 nm

The spontaneous emission and gain characteristics of both two-layer and three-layer staggered InGaN QW designed for lasing wavelength at ~500 nm are compared to those of conventional InGaN QW. Figure 10 shows the band lineups for (a) conventional 30-Å $In_{0.3}Ga_{0.7}N$ QW, (b) two-layer staggered 20-Å $In_{0.33}Ga_{0.67}N$/10-Å $In_{0.17}Ga_{0.83}N$ QW, and (c) three-layer staggered 5-Å $In_{0.17}Ga_{0.83}N$/20-Å $In_{0.33}Ga_{0.67}N$/5-Å $In_{0.17}Ga_{0.83}N$ QW at carrier density $n=7\times10^{19}$ cm^{-3}. The QW structures were chosen with similar thickness for comparison purpose. The emission wavelengths of the peak gain for all three QWs structures are relatively similar at low carrier density, however the significant larger carrier screening effect in conventional InGaN QW leads to slightly shorter lasing wavelength ($\lambda\sim480$ nm) in comparison to that of the staggered InGaN QWs ($\lambda\sim500$ nm) at near threshold gain ($g_{th}=1500$ cm^{-1}). Note that the threshold gain ($g_{th}=1500$ cm^{-1}) employed in the analysis for green-emitting nitride lasers is similar to that of laser structures described in Sec. IV C.

Figure 11 shows the calculated spontaneous emission spectra for conventional InGaN QW, two-layer staggered InGaN QW and three-layer staggered InGaN QW at carrier densities of $n=3-7\times10^{19}$ cm^{-3} at T=300 K. Note that a second peak of the spontaneous emission spectrum appears when the carrier density increases to $n=5\times10^{19}$ cm^{-3} due to the transitions between higher energy states of the conduction subbands and valence subbands. The second peak will

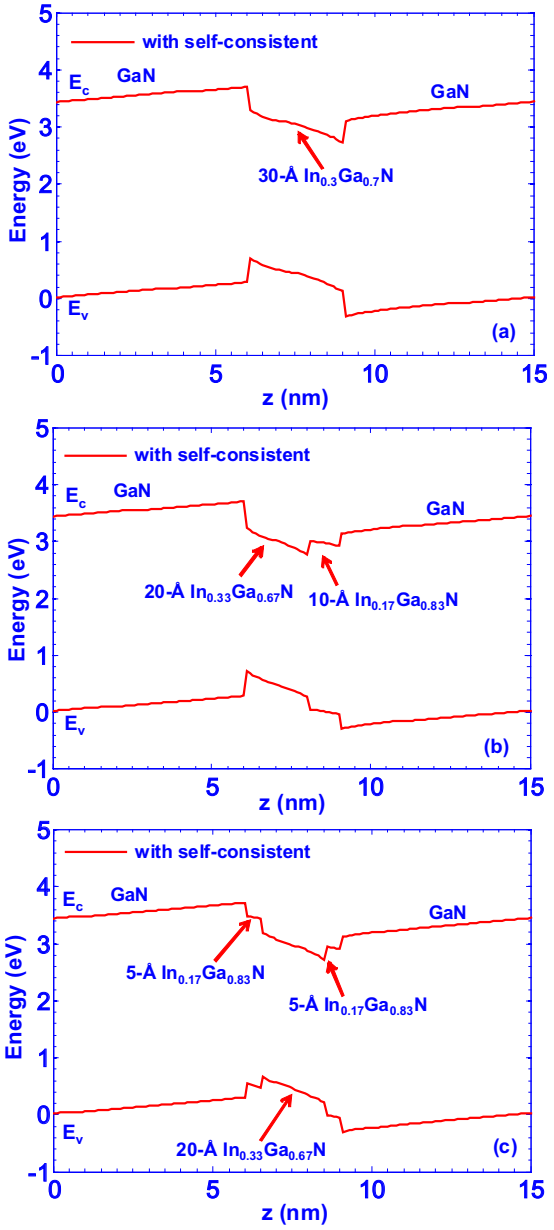

FIG. 10. (Color online) Energy band lineups of (a) 24-Å $In_{0.22}Ga_{0.78}N$ QW, (b) two-layer staggered 20-Å $In_{0.33}Ga_{0.67}N$/10-Å $In_{0.17}Ga_{0.83}N$ QW, and (c) three-layer staggered 5-Å $In_{0.17}Ga_{0.83}N$/20-Å $In_{0.33}Ga_{0.67}N$/5-Å $In_{0.17}Ga_{0.83}N$ QW at carrier density $n=7\times10^{19}$ cm^{-3}. The calculations are based on a self-consistent 6-band $\boldsymbol{k}\cdot\boldsymbol{p}$ method.

become more obvious as the carrier density increases. At $n=7\times10^{19}$ cm^{-3}, the second peak of the spontaneous emission spectrum of the conventional InGaN QW becomes higher than the dominant peak of the spontaneous emission spectrum ($n=1$, $m=1$).

As shown in Fig. 12, the spontaneous emission spectra for both two-layer staggered and three-layer staggered InGaN QWs are significantly enhanced as compared to that of the conventional InGaN QW. At $n=5\times10^{19}$ cm^{-3}, the two-layer (and three-layer) staggered InGaN QW shows approximately 1.93 times (and 2.12 times) higher in the peak of the spontaneous emission spectra than that of the conventional InGaN QW.

Figure 12 illustrates the spontaneous emission radiative recombination rate per unit volume (R_{sp}) for the conventional InGaN QW, the two-layer staggered InGaN QW and the three-layer staggered InGaN QW as a function of the carrier density up to 7×10^{19} cm^{-3}. For the two-layer staggered InGaN QW, the enhancement of the spontaneous emission radiative recombination rate (R_{sp}) as a function of carrier density ranges between 1.44–2.72 times as compared to the conventional InGaN QW. The R_{sp} for the three-layer staggered InGaN QW as a function of carrier density exhibited enhancement of 1.48–3.27 times, in comparison to that of the conventional InGaN QW.

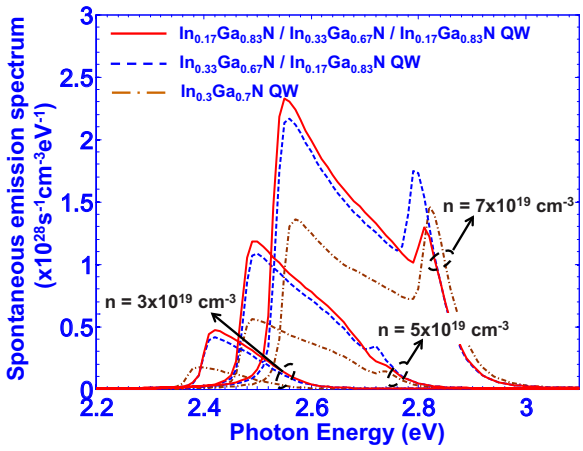

FIG. 11. (Color online) Spontaneous emission spectra for conventional 30-Å $In_{0.3}Ga_{0.7}N$ QW, two-layer staggered 20-Å $In_{0.33}Ga_{0.67}N$/10-Å $In_{0.17}Ga_{0.83}N$ QW and three-layer staggered 5-Å $In_{0.17}Ga_{0.83}N$/20-Å $In_{0.33}Ga_{0.67}N$/5-Å $In_{0.17}Ga_{0.83}N$ QW for increasing carrier density $n=3-7\times10^{19}$ cm^{-3}.

Figure 13 shows the optical gain spectra for the conventional InGaN QW (dashed-dotted line), two-layer staggered InGaN QW (dashed line), and three-layer staggered InGaN QW (solid line) at various carrier densities ($n=3\times10^{19}$ cm^{-3}, 5×10^{19} cm^{-3}, and 7×10^{19} cm^{-3}) at T=300 K. The staggered InGaN QWs exhibit improved optical gain as compared to the conventional InGaN QW. At $n=7\times10^{19}$ cm^{-3}, the peak gain (g_p) for the two-layer staggered InGaN QW is 2150 cm^{-1}, which is 1.6 times of that of

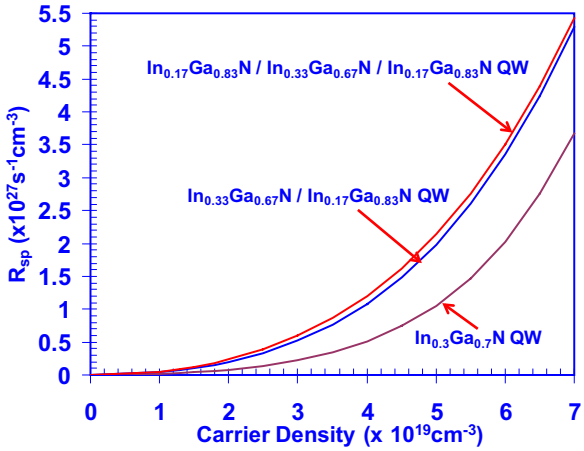

FIG. 12. (Color online) Spontaneous emission radiative recombination rate (R_{sp}) as a function of carrier density for conventional 30-Å $In_{0.3}Ga_{0.7}N$ QW, two-layer staggered 20-Å $In_{0.33}Ga_{0.67}N$/10-Å $In_{0.17}Ga_{0.83}N$ QW and three-layer staggered 5-Å $In_{0.17}Ga_{0.83}N$/20-Å $In_{0.17}Ga_{0.83}N$/5-Å $In_{0.17}Ga_{0.83}N$ QW at room temperature.

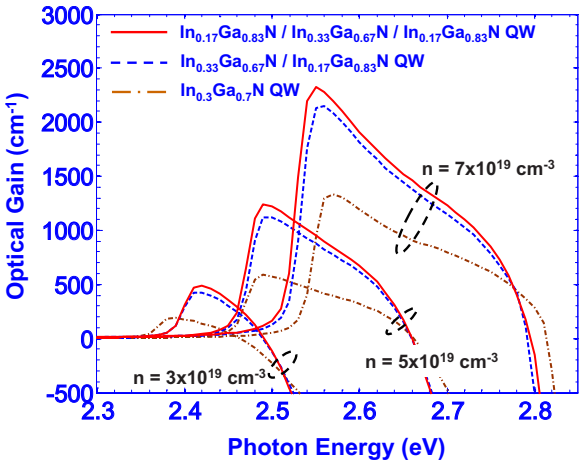

FIG. 13. (Color online) Optical gain spectra for conventional 30-Å $In_{0.3}Ga_{0.7}N$ QW, two-layer staggered 20-Å $In_{0.33}Ga_{0.67}N$/10-Å $In_{0.17}Ga_{0.83}N$ QW and three-layer staggered 5-Å $In_{0.17}Ga_{0.83}N$/20-Å $In_{0.17}Ga_{0.83}N$/5-Å $In_{0.17}Ga_{0.83}N$ QW emitting at ~440-nm for increasing carrier density $n = 3-7\times10^{19}$ cm^{-3}.

the conventional InGaN QW (1340 cm^{-1}), while the three-layer staggered InGaN QW shows 1.74 times improvement with peak gain of 2330 cm^{-1}. Note that at the carrier density $n=7\times10^{19}$ cm^{-3}, the gain spectra show the contribution from the excited state transitions from the band filling effects. However, the band filling effect is more dominant for conventional InGaN QW, in comparison to those of both staggered InGaN QW structures.

Figure 14 shows the peak material gain of the three QW structures as a function of carrier density up to 7×10^{19} cm^{-3}. A significant enhancement in the peak material gain (g_p) by utilizing the staggered InGaN QW structures is observed in Fig. 14, which is important for reducing the threshold carrier density (n_{th}) for nitride lasers emitting in the green spectral regime. Note that the three structures have similar transparency carrier density (n_{tr}) ~ 1.4×10^{19} cm^{-3}. The two-layer staggered InGaN QW shows 1.6–2.5 times enhancement in peak material gain as compared to that of the conventional InGaN QW, while the enhancement in three-layer staggered InGaN QW shows 1.75–3.0 times for various carrier densities studied here.

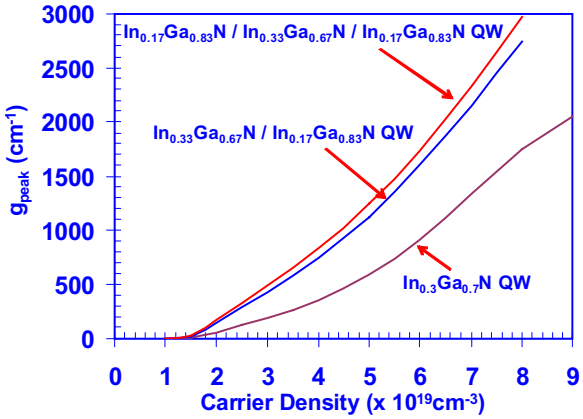

FIG. 14. (Color online) Peak optical gain (g_p) as a function of carrier density for conventional 30-Å $In_{0.3}Ga_{0.7}N$ QW, two-layer staggered 20-Å $In_{0.33}Ga_{0.67}N$/10-Å $In_{0.17}Ga_{0.83}N$ QW and three-layer staggered 5-Å $In_{0.17}Ga_{0.83}N$/20-Å $In_{0.17}Ga_{0.83}N$/5-Å $In_{0.17}Ga_{0.83}N$ QW at room temperature.

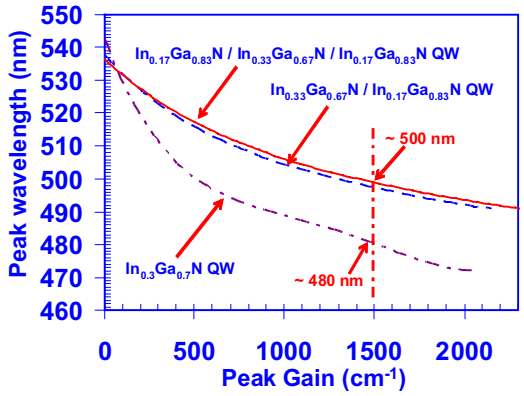

FIG. 15. (Color online) Peak emission wavelengths from the gain spectra as a function of material gain for conventional 30-Å $In_{0.3}Ga_{0.7}N$ QW, two-layer staggered 20-Å $In_{0.33}Ga_{0.67}N$/10-Å $In_{0.17}Ga_{0.83}N$ QW and three-layer staggered 5-Å $In_{0.17}Ga_{0.83}N$/20-Å $In_{0.17}Ga_{0.83}N$/5-Å $In_{0.17}Ga_{0.83}N$ QW.

From the results presented in Fig. 14, the use of conventional InGaN QW leads to significant challenges to achieve the threshold lasing condition (for $g_{th}=1500$ cm^{-1}) in the green spectral regime due to the low optical gain. By utilizing the staggered InGaN QW structure with improved overlap, the optical gain characteristics is significantly enhanced, which leads to significantly reduced threshold carrier density. As shown in Fig. 14, the threshold carrier densities for the two-layer and three-layer staggered InGaN QWs (for $g_{th}=1500$ cm^{-1}) are $n_{th}=5.5\times10^{19}$ cm^{-3} and $n_{th}=5.2\times10^{19}$ cm^{-3}, respectively, for lasing wavelength at λ_{lasing} ~ 500 nm. The conventional InGaN QW requires higher threshold carrier density ($n_{th}\sim7.4\times10^{19}$ cm^{-3}) to reach the lasing condition of $g_{th}=1500$ cm^{-1}, with significantly shorter lasing wavelength ($\lambda_{lasing}\sim480$ nm) due to the stronger carrier screening effect.

The gain saturation is observed for conventional InGaN QW at high carrier density ($n>8\times10^{19}$ cm^{-3}) due to the broadening of the gain spectrum, while the gain characteristics for both staggered InGaN QWs do not exhibit the saturation profile at this carrier density. To achieve higher material gain ($g=2050$ cm^{-1}), the carrier density required in conventional InGaN QW is $n=9.0\times10^{19}$ cm^{-3}, while the three-layer (and two-layer) staggered InGaN QW requires carrier density of only $n=6.6\times10^{19}$ cm^{-3} ($n=6.8\times10^{19}$ cm^{-3}). The challenges for the conventional InGaN QW to achieve low-threshold green nitride lasers can be attributed to (1) significant carrier screening due to the higher threshold carrier density in the QW, which leads to significant blueshift in lasing wavelength; (2) the carrier filling effect leads to strong transition from excited states, which leads to broadened gain spectrum at high carrier density.

D. Threshold current density for staggered InGaN QWs lasers at 500 nm

Figure 15 shows the peak emission wavelength versus the material gain for the conventional, the two-layer staggered and the three-layer staggered InGaN QWs. As the optical gain increases, the peak emission wavelengths show blueshift for all three structures. The staggered InGaN QWs show significantly-less blueshift as compared to that of the

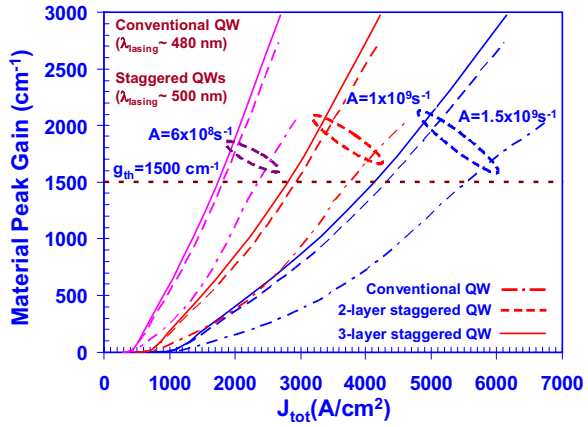

FIG. 16. (Color online) Material gain vs. total current density for conventional 30-Å $In_{0.3}Ga_{0.7}N$ QW, two-layer staggered 20-Å $In_{0.33}Ga_{0.67}N$/10-Å $In_{0.17}Ga_{0.83}N$ QW and three-layer staggered 5-Å $In_{0.17}Ga_{0.83}N$/20-Å $In_{0.17}Ga_{0.83}N$/5-Å $In_{0.17}Ga_{0.83}N$ QW with monomolecular recombination rate of $A=6\times10^8$ s^{-1}, 1×10^9 s^{-1}, and 1.5×10^9 s^{-1}.

conventional InGaN QW. Note the lasing wavelength for both staggered InGaN QWs is ~500 nm for threshold gain (g_{th})=1500 cm^{-1}, while the lasing wavelength for the conventional InGaN QW is blueshifted to ~480 nm. The extension of the lasing wavelength to 500 nm for both staggered InGaN QWs is attributed to the enhanced electron-hole wave functions overlap and improved optical gain, which leads to the reduced carrier screening. At higher material gain (g =2000 cm^{-1}), the emission wavelengths for both staggered QW designs are at ~497 nm, while the emission wavelength for conventional QW is significantly blueshifted to ~472 nm.

Figure 16 shows the peak material gain (g_p) as a function of the total threshold current density ($J_{tot}=J_{rad}+J_{nr}$) for the two-layer staggered 20-Å $In_{0.33}Ga_{0.67}N$/10-Å $In_{0.17}Ga_{0.83}N$ QW and three-layer staggered 5-Å $In_{0.17}Ga_{0.83}N$/20-Å $In_{0.33}Ga_{0.67}N$/5-Å $In_{0.17}Ga_{0.83}N$ QW with three different monomolecular recombination rates ($A=5\times10^8$ s^{-1}, $A=1\times10^9$ s^{-1}, and $A=1.5\times10^9$ s^{-1}). To achieve the threshold condition (g_{th}=1500 cm^{-1}), the required total threshold current densities for the two-layer staggered InGaN QW and three-layer staggered InGaN QW at three different monomolecular recombination rate are shown in Table II. The threshold carrier density for three-layer (or two-layer) staggered InGaN QW is reduced by 30% (or 26%) in comparison to that of conventional InGaN QW (λ_{lasing}~480 nm), which in turn leads to 25.7%–28.5% (and 20%–24.3%) reduction in threshold current density for three-layer (or two-layer) staggered InGaN QW lasers (λ_{lasing} ~500 nm). Note that the improvement observed in threshold characteristic in staggered InGaN QW structures is accompanied by the ~20 nm longer lasing emission wavelength, which is attributed to the much reduced threshold carrier density and less carrier screening in the staggered QWs. The improvement observed in staggered InGaN QW lasers is attributed to the higher electron-hole wave function overlap for the QW structures. If Auger recombination process is taken into account, the reduction in threshold carrier density will lead to reduction in Auger recombination current density (J_{th_Auger}) by 66% (or 59%) for three-layer (or two-layer) staggered InGaN QW.

Thus, the use of InGaN-based QW designs with improved electron-hole wave function overlap (i.e., staggered InGaN QW) is important to enable significant reduction in threshold current density in green-emitting nitride LDs. Two important features in the InGaN QW design with improved overlap (Γ_{e_hh}) to ensure the advantages offered by such active region are as follows: (1) significant reduction in threshold carrier density for achieving reduction in blueshift and nonradiative recombination current and (2) large optical matrix element to minimize the effect from band filling from excited states transitions. The use of two-layer or three-layer staggered InGaN QW is promising for enabling low-threshold lasers in the green spectral regime.

Note that the current model do not take into consideration the influence of the exciton binding energy on the optical gain and threshold current density. Due to the enhanced electron-hole wave function overlap, the exciton binding energy for the staggered InGaN QWs will be slightly higher than the conventional InGaN QW,[45] which causes the broadening of the optical gain spectrum as well as the increase of the threshold current density. However, the effect from the exciton binding energy is expected to be negligible due to the large carrier screening effect on the column interaction between electron-hole pairs in III-Nitride LDs operating at high carrier density.[44,45]

VI. SUMMARY

In summary, staggered InGaN QWs are analyzed as the improved gain media for LDs emitting at ~440 nm and ~500 nm. Both two-layer and three-layer staggered InGaN

TABLE II. Total threshold current densities (J_{th_total}) for conventional InGaN QW (30-Å $In_{0.3}Ga_{0.7}N$), two-layer staggered InGaN QW (20-Å $In_{0.33}Ga_{0.67}N$/10-Å $In_{0.17}Ga_{0.83}N$) and three-layer staggered InGaN QW (5-Å $In_{0.17}Ga_{0.83}N$/20-Å $In_{0.33}Ga_{0.67}N$/5-Å $In_{0.17}Ga_{0.83}N$ QW) with various monomolecular recombination rates (A). The staggered InGaN QW lasers have lasing wavelength at ~500 nm, while the lasing wavelength of conventional InGaN QW is ~480 nm.

	Total threshold current density (J_{th_total}) (A/cm^2)		
Monomolecular recombination coefficient (A)	Conventional InGaN QW	Two-layer staggered InGaN QW	Three-layer staggered InGaN QW
$A=6\times10^8$ s^{-1}	2390	1810	1710
$A=1\times10^9$ s^{-1}	3800	2920	2800
$A=1.5\times10^9$ s^{-1}	5530	4420	4110
Lasing wavelength	480 nm	500 nm	500 nm

QWs are designed with improved electron-hole wave function overlap to enhance the spontaneous emission radiative recombination rate and optical gain. The analysis of the band structures was carried out based on a self-consistent 6-band $\boldsymbol{k}\cdot\boldsymbol{p}$ method for wurtzite semiconductor taking into account the valence band mixing, strain effect, spontaneous, and piezoelectric polarizations, and carrier screening effect. The analysis indicated that the optical gain for three-layer (and two-layer) staggered InGaN QWs are enhanced by 1.5–2.35 times (and 1.3–1.75 times) in comparison to that of conventional InGaN QW emitting at ~440 nm, which leads to significant reduction in threshold carrier density by 25% (and 15%) in the staggered QW designs. At $n=5\times10^{19}$ cm^{-3}, the peak gain for the three-layer (and two-layer) staggered InGaN QW is enhanced by 1.61 times (and 1.34 times) of that of the conventional InGaN QW. The reduction in threshold current density by 23.5%–23.8% (and 15.7%–17%) is expected for blue-emitting lasers employing three-layer (and two-layer) staggered InGaN QW as gain media.

Note that the analysis presented here employed the 6-band $\boldsymbol{k}\cdot\boldsymbol{p}$ method, which is widely used for the calculation of nitride based QWs (ie. staggered InGaN QW,[19,20,22] InGaN QW with embedded δ-AlGaN layer,[11,12] dip-shaped InGaN QW,[21] triangular shape QW,[27] and nonpolar InGaN QW (Ref. 10)]. However, it is also important to point out the limitation of the 6-band $\boldsymbol{k}\cdot\boldsymbol{p}$ model in computing the band structure properties for QW structure with thin sublayers, due to the less accuracy of the envelope function theory for structures with ultrathin layers. Nevertheless, this approach allows us to provide the comparison of the trends for the optoelectronics properties of the QW structures. The use of tight-binding atomistic approach,[46,47] plane-wave pseudopotentials,[48] or first principle density functional theory (DFT) (Refs. 49 and 50) are required in order to provide more accurate band structure of the nanostructures with ultrathin layers.

The use of conventional InGaN QW as green-emitting nitride laser active regions suffers from the significantly reduced electron-hole wave function overlap. The poor overlap in the conventional InGaN QW leads to significantly higher threshold carrier density and strong carrier screening effect, which leads to high threshold current density and strong blueshift in lasing wavelength. The peak gain of green-emitting three-layer (and two-layer) staggered InGaN QWs are enhanced by 1.75–3 times (and 1.6–2.5 times) as compared to that of conventional InGaN QW. The use of three-layer (and two-layer) staggered InGaN QW as the laser active region at $\lambda\sim500$ nm leads to significant reduction in threshold carrier density by 30% (and 26%), which leads to reduction in threshold current density of 25.7%–28.5% (and 20%–24.3%) in comparison to that of conventional QW ($\lambda_{lasing}\sim480$ nm). The use of InGaN-based QW with improved electron-hole wave function overlap (i.e., staggered InGaN QW) is important for achieving low-threshold and reliable nitride lasers emitting in the green spectral regime and beyond.

ACKNOWLEDGMENTS

The authors acknowledge support from National Science Foundation (Grant No. ECCS#0701421), U.S. Department of Energy (Grant No. DE-FC26-08NT01581), and P. C. Rossin Professorship Funds.

[1] S. Nakamura, M. Senoh, S. Nagahama, N. Iwasa, T. Matsushita, and T. Mukai, Appl. Phys. Lett. **76**, 22 (2000).
[2] H. Y. Ryu, K. H. Ha, S. N. Lee, T. Jang, H. K. Kim, J. H. Chae, K. S. Kim, K. K. Choi, J. K. Son, H. S. Paek, Y. J. Sung, T. Sakong, O. H. Nam, and Y. J. Park, Appl. Phys. Lett. **89**, 031122 (2006).
[3] H. Y. Ryu, K. H. Ha, S. N. Lee, T. Jang, J. K. Son, H. S. Paek, Y. J. Sung, H. K. Kim, K. S. Kim, O. H. Nam, Y. J. Park, and J. I. Shim, IEEE Photon. Technol. Lett. **19**, 1717 (2007).
[4] N. Tansu, J. Y. Yeh, and L. J. Mawst, Appl. Phys. Lett. **82**, 4038 (2003).
[5] N. Tansu and L. J. Mawst, J. Appl. Phys. **97**, 054502 (2005).
[6] I. H. Brown, P. Blood, P. M. Smowton, J. D. Thomson, S. M. Olaizola, A. M. Fox, P. J. Parbrook, and W. W. Chow, IEEE J. Quantum Electron. **42**, 1202 (2006).
[7] Y. J. Sun, O. Brandt, S. Cronenberg, S. Dhar, H. T. Grahn, K. H. Ploog, P. Waltereit, and J. S. Speck, Phys. Rev. B **67**, 041306 (2003).
[8] A. Chakraborty, B. A. Haskell, S. Keller, J. S. Speck, S. P. DenBaars, S. Nakamura, and U. K. Mishraa, Appl. Phys. Lett. **85**, 5143 (2004).
[9] K. Okamoto, H. Ohta, S. F. Chichibu, J. Ichihara, and H. Takasu, Jpn. J. Appl. Phys., Part 2 **46**, L187 (2007).
[10] S. H. Park, D. Ahn, and S. L. Chuang, IEEE J. Quantum Electron. **43**, 1175 (2007).
[11] J. Park and Y. Kawakami, Appl. Phys. Lett. **88**, 202107 (2006).
[12] S. H. Park, J. Park, and E. Yoon, Appl. Phys. Lett. **90**, 023508 (2007).
[13] R. A. Arif, Y.-K. Ee, and N. Tansu, Appl. Phys. Lett. **91**, 091110 (2007).
[14] R. A. Arif, H. Zhao, Y.-K. Ee, and N. Tansu, IEEE J. Quantum Electron. **44**, 573 (2008).
[15] R. A. Arif, Y.-K. Ee, and N. Tansu, Phys. Stat. Sol. A, **205**, 96 (2008).
[16] H. Zhao, R. A. Arif, and N. Tansu, IEEE J. Sel. Top. Quantum Electron. **15**, 1104 (2009).
[17] H. Zhao, G. Liu, X. H. Li, G. S. Huang, J. D. Poplawsky, S. Tafon Penn, V. Dierolf, and N. Tansu, Appl. Phys. Lett. **95**, 061104 (2009).
[18] H. P. Zhao, G. Y. Liu, X. H. Li, R. A. Arif, G. S. Huang, J. D. Poplawsky, S. Tafon Penn, V. Dierolf, and N. Tansu, IET Optoelectronics **3**, 283 (2009).
[19] S. H. Park, D. Ahn, and J. W. Kim, Appl. Phys. Lett. **94**, 041109 (2009).
[20] S. H. Park, D. Ahn, B. H. Koo, and J. W. Kim, Phys. Stat. Sol. A **206**, 2637 (2009).
[21] S. H. Park, D. Ahn, B. H. Koo, and J. W. Kim, Appl. Phys. Lett. **95**, 063507 (2009).
[22] S. H. Yen and Y. K. Kuo, Opt. Commun. **281**, 4735 (2008).
[23] R. A. Arif, H. Zhao, and N. Tansu, Appl. Phys. Lett. **92**, 011104 (2008).
[24] H. Zhao, R. A. Arif, and N. Tansu, J. Appl. Phys. **104**, 043104 (2008).
[25] H. Zhao, R. A. Arif, Y. K. Ee, and N. Tansu, Opt. Quantum Electron. **40**, 301 (2008).
[26] H. Zhao, R. A. Arif, Y. K. Ee, and N. Tansu, IEEE J. Quantum Electron. **45**, 66 (2009).
[27] Z. Yang, R. Li, Q. Wei, T. Yu, Y. Zhang, W. Chen, and X. Hu, Appl. Phys. Lett. **94**, 061120 (2009).
[28] S. L. Chuang, IEEE J. Quantum Electron. **32**, 1791 (1996).
[29] S. L. Chuang and C. S. Chang, Semicond. Sci. Technol. **12**, 252 (1997).
[30] S. L. Chuang, *Physics of Photonic Devices* 2nd ed. (Wiley, New York, 2009), Chap. 4.
[31] I. Vurgaftman and J. R. Meyer, in *Nitride Semiconductor Devices*, edited by J. Piprek (Wiley-CCH, Weinheim, 2007), Chap. 2.
[32] I. Vurgaftman and J. R. Meyer, J. Appl. Phys. **94**, 3675 (2003).
[33] J. Hader, J. V. Moloney, A. Thranhardt, and S. W. Koch, in *Nitride Semiconductor Devices*, edited by J. Piprek (Wiley-CCH, Weinheim, 2007), Chap. 7.
[34] J. Hader, J. V. Moloney, B. Pasenow, S. W. Koch, M. Sabathil, N. Linder, and S. Lutgen, Appl. Phys. Lett. **92**, 261103 (2008).
[35] W. W. Chow and M. Kneissl, J. Appl. Phys. **98**, 114502 (2005).
[36] Y. C. Shen, G. O. Mueller, S. Watanabe, N. F. Gardner, A. Munkholm, and M. R. Krames, Appl. Phys. Lett. **91**, 141101 (2007).
[37] K. T. Delaney, P. Rinke, and C. G. Van de Walle, Appl. Phys. Lett. **94**, 191109 (2009).
[38] T. Miyoshi, S. Masui, T. Okada, T. Yanamoto, T. Kozaki, S. Nagahama,

and T. Mukai, Appl. Phys. Express **2**, 062201 (2009).
[39]D. Queren, A. Avramescu, G. Bruderl, A. Breidenassel, M. Schillgalies, S. Lutgen, and U. Strauß, Appl. Phys. Lett. **94**, 081119 (2009).
[40]W. W. Chow, H. Amano, T. Takeuchi, and J. Han, Appl. Phys. Lett. **75**, 244 (1999).
[41]L. H. Peng, Y. C. Hsu, and C. W. Chuang, IEEE J. Sel. Top. Quantum Electron. **5**, 756 (1999).
[42]W. W. Chow, O. B. Spahn, H. C. Schneider, and J. F. Klem, IEEE J. Quantum Electron. **37**, 1178 (2001).
[43]J. D. Thomson, P. M. Smowton, P. Blood, and J. F. Klem, IEEE J. Quantum Electron. **43**, 607 (2007).
[44]G. Traetta, R. Cingolani, A. D. Carlo, F. D. Sala, and P. Lugli, Appl. Phys. Lett. **76**, 1042 (2000).
[45]U. M. E. Christmas, A. D. Andreev, and D. A. Faux, J. Appl. Phys. **98**, 073522 (2005).
[46]X. Guan and Z. Yu, IEEE Trans. Nanotechnol. **6**, 101 (2007).
[47]M. Korkusinski, G. Klimeck, H. Xu, S. Lee, S. Goasguen, and F. Saied, Proceedings of 2005 NSTI Conference, Anaheim, CA (2005).
[48]W. B. Jones, G. Bester, A. Canning, A. Franceschetti, P. A. Graf, K. Kim, J. Langou, L. W. Wang, J. Dongarra, and A. Zunger, J. Phys.: Conf. Ser. **16**, 277 (2005).
[49]R. M. Martin, *Electronic Structure: Basic Theory and Practical Methods* (Cambridge University Press, Cambridge, 2004).
[50]C. G. Van de Walle and J. Neugebauer, J. Appl. Phys. **95**, 3851 (2004).